The 3 × 120° rotary mechanism of *Paracoccus denitrificans* F_1-ATPase is different from that of the bacterial and mitochondrial F_1-ATPases

Mariel Zarco-Zavala[a,1], Ryo Watanabe[a], Duncan G. G. McMillan[b], Toshiharu Suzuki[c], Hiroshi Ueno[a], Francisco Mendoza-Hoffmann[d], José J. García-Trejo[d,1], and Hiroyuki Noji[a,1]

[a]Department of Applied Chemistry, Graduate School of Engineering, The University of Tokyo, 113-8656 Tokyo, Japan; [b]Department of Biotechnology, Delft University of Technology, 2629 HZ Delft, the Netherlands; [c]Laboratory for Chemistry and Life Science, Institute of Innovative Research, Tokyo Institute of Technology, 226-8503 Yokohama, Japan; and [d]Department of Biology, Chemistry Faculty, National Autonomous University of Mexico, 04510 Mexico City, Mexico

Edited by Martin Karplus, Harvard University, Cambridge, MA, and approved October 9, 2020 (received for review February 26, 2020)

The rotation of *Paracoccus denitrificans* F_1-ATPase (PdF_1) was studied using single-molecule microscopy. At all concentrations of adenosine triphosphate (ATP) or a slowly hydrolyzable ATP analog (ATPγS), above or below K_m, PdF_1 showed three dwells per turn, each separated by 120°. Analysis of dwell time between steps showed that PdF_1 executes binding, hydrolysis, and probably product release at the same dwell. The comparison of ATP binding and catalytic pauses in single PdF_1 molecules suggested that PdF_1 executes both elementary events at the same rotary position. This point was confirmed in an inhibition experiment with a nonhydrolyzable ATP analog (AMP-PNP). Rotation assays in the presence of adenosine diphosphate (ADP) or inorganic phosphate at physiological concentrations did not reveal any obvious substeps. Although the possibility of the existence of substeps remains, all of the datasets show that PdF_1 is principally a three-stepping motor similar to bacterial vacuolar (V_1)-ATPase from *Thermus thermophilus*. This contrasts with all other known F_1-ATPases that show six or nine dwells per turn, conducting ATP binding and hydrolysis at different dwells. Pauses by persistent Mg-ADP inhibition or the inhibitory ζ-subunit were also found at the same angular position of the rotation dwell, supporting the simplified chemomechanical scheme of PdF_1. Comprehensive analysis of rotary catalysis of F_1 from different species, including PdF_1, suggests a clear trend in the correlation between the numbers of rotary steps of F_1 and F_o domains of F-ATP synthase. F_1 motors with more distinctive steps are coupled with proton-conducting F_o rings with fewer proteolipid subunits, giving insight into the design principle the F_1F_o of ATP synthase.

F_1-ATPase | rotation | single-molecule analysis | ζ-subunit

F_1F_o-ATP synthase (or F-ATP synthase) is nature's smallest rotary motor and produces most of a cell's chemical energy in the form of adenosine triphosphate (ATP). Powered by a transmembrane electrochemical ion gradient, this enzyme catalyzes the synthesis of ATP from adenosine diphosphate (ADP) and inorganic phosphate (P_i) (1). F-ATP synthase is composed of two rotary molecular motors, named as F_1 and F_o. Water-soluble F_1 catalyzes the synthesis (when complexed with F_o) or hydrolysis of ATP, and membrane-embedded F_o conducts translocation of H^+ or Na^+ ions (2) across the membrane (3–5). F_1 and F_o form the whole complex of F-ATP synthase, connecting together via a central and a peripheral stalk (6).

F_1 (also known as F_1-ATPase) remains catalytically active as an ATPase when it is isolated from F_o, and its rotary catalysis mechanism has been widely studied. F_1 is composed of a hexameric catalytic core, formed by $\alpha_3\beta_3$-subunits, that surrounds a central rotary shaft formed by a γ/ε-subcomplex (7, 8). Each α/β-interface in the $\alpha_3\beta_3$-ring has a catalytic reaction center, while most of catalytic residues reside on the β-subunit. The three β-subunits exhibit significant differences in their affinity for Mg^{2+} nucleotides, adopting three functionally distinct conformations. Each conformational state of the β-subunit is designated as β_T, β_D, or β_E (8, 9).

Single-molecule and biochemical studies have established that hydrolysis of ATP by F_1 or F_1F_o produces continuous rotation of the central shaft in a counterclockwise (CCW) direction when viewed from the membrane (10). The rotation results from the repetition of discrete 120° cycles in which the three β-subunits cooperatively change their conformation and one ATP molecule is consumed (11).

Extensive single-molecule studies from the *Bacillus* strain *PS3* F_1 (TF_1) (10, 12–14) elucidated a detailed chemomechanical coupling mechanism of a bacterial enzyme (Fig. 1*A*) that was later supported by the description of the *Escherichia coli* F_1 (EF_1) (15–19). In these bacterial enzymes, each 120° cycle is further divided into two substeps, resulting in six intervening dwells per turn. An 80°–85° substep is triggered by ATP binding and the concurrent ADP release that occurs on two different β-subunits, and another 40°–35° substep is initiated after ATP cleavage and triggered by the release of P_i, which occurs

Significance

F-ATP synthase is a fundamental enzyme supplying adenosine triphosphate (ATP), spreading across all kingdoms of life. Despite remarkable conservation of its basic structure and function, biophysical studies have revealed discrete differences in the rotary mechanisms of bacterial and eukaryotic F_1-ATPases (the catalytic portions of the enzymes). Here, we analyzed the rotational dynamics of *Paracoccus denitrificans* F_1 (PdF_1), a bacterial F_1-ATPase that exhibits high homology with the core functional subunits of its mitochondrial counterpart. Notably, PdF_1 possesses a simplified chemomechanical scheme different from that of all other F_1-ATPases. Our results reveal an unexpected diversity in the chemomechanical coupling cycle of the F_1-ATPase machinery and show that features such as homology or phylogenetic relationship cannot uniquely define the rotary scheme pattern.

Author contributions: M.Z.-Z., D.G.G.M., T.S., H.U., J.J.G.-T., and H.N. designed research; M.Z.-Z., R.W., and F.M.-H. performed research; J.J.G.-T. and H.N. contributed new reagents/analytic tools; M.Z.-Z. and R.W. analyzed data; and M.Z.-Z. wrote the paper.

The authors declare no competing interest.

This article is a PNAS Direct Submission.

[1]To whom correspondence may be addressed. Email: marielzarco_zavala@comunidad.unam.mx, jjgartre@unam.mx, or hnoji@g.ecc.u-tokyo.ac.jp.

This article contains supporting information online at https://www.pnas.org/lookup/suppl/doi:10.1073/pnas.2003163117/-/DCSupplemental.

First published November 9, 2020.

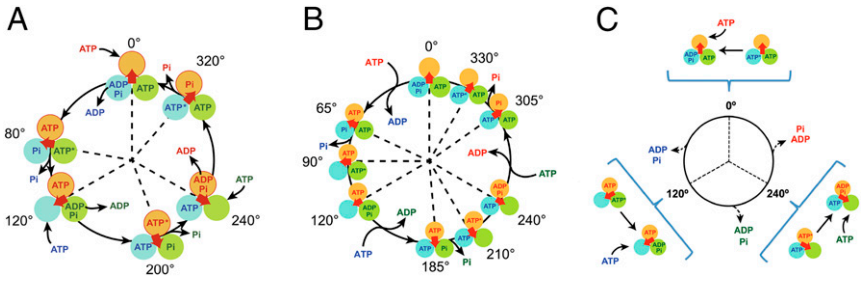

Fig. 1. Proposed chemomechanical coupling schemes of the (*A*) bacterial TF_1, (*B*) eukaryotic hMF_1, and (*C*) PdF_1. In all images, each circle represents the chemical state of the catalytic site in each β-subunit, the central red arrow represents the orientation of the γ-subunit, ATP* represents the prehydrolysis state of ATP, and 0° is defined as the ATP binding angle for the catalytic site at the 12 o'clock position. In *C*, dashed arrows indicate that the simultaneous release of P_i and ADP has not yet been precisely determined.

sequentially at two different β-subunits. The dwells before the 80°–85° and 40°–35° substeps are referred to as binding and catalytic dwells, respectively.

Mitochondrial F_1 exhibits a variety of chemomechanical coupling schemes different from that of its bacterial counterpart (20–23). Human mitochondrial F_1 (hMF_1) (Fig. 1*B*) and bovine mitochondrial F_1 (bMF_1) exhibit a chemomechanical coupling scheme in which each 120° cycle is composed of three substeps, and nine intervening pauses form one revolution (20, 21). Both enzymes display two intervening dwells associated with catalytic and binding states (with an angular displacement of 90° for hMF_1 and 80° for bMF_1) in addition to a third intervening pause (located at 65° from the binding dwell in hMF_1 and 10°–20° in bMF_1). Single-molecule studies and crystallographic evidence have associated the third intervening pause in hMF_1 with a pre-P_i release state (21, 24). However, the identity of the catalytic state that is associated with the third dwell in the case of bMF_1 remains elusive (20).

Despite its high homology, the rotation dynamics of *Saccharomyces cerevisiae* F_1 (YMF_1) (22) show several differences from other mitochondrial F_1's. Consistent with all F_1-ATPases, this enzyme displays two clear intervening pauses associated with catalytic and binding states. However, no clear evidence of a third intervening dwell has been uncovered.

Since the minimal F_1 structural morphology remains conserved among bacteria and mitochondrial enzymes, the differences between their chemomechanical mechanisms may suggest adaptation and/or additional undescribed function(s). To gain insight into the understanding of these differences, we studied the mechanical properties of the F_1-ATPase of the α-proteobacterium *Paracoccus denitrificans* (Pd), a bacterial model organism used in the bioenergetic field to study eukaryotic respiratory enzymes. This organism has been proposed to have common ancestry with mitochondria (25), and its respiratory chain has many similarities with the mitochondrial one.

PdF_1F_o-ATPase has a canonical bacterial composition and high amino acid conservation with the core functional subunits of its mitochondrial counterpart (26). Biochemical studies showed that this enzyme exhibits tightly regulated slow ATP hydrolysis activity and high ATP synthase activity (27–29). The inhibition of ATP hydrolysis involves an inhibitor protein known as the ζ-subunit, which is exclusively conserved in the alphaproteobacteria class (30). The ζ-subunit possesses a structure different from the other known bacterial and mitochondrial regulatory subunits (ε-subunit and ATPase inhibitory factor 1 [IF_1]) (31). Still, the sequence of its inhibitory region is weakly related to that of the mitochondrial inhibitor IF_1 (32). Biochemical and crystallographic evidence supports the notion that the ζ-inhibitory mechanism resembles that of IF_1, in which the ζ-intrinsically disordered inhibitory domain adopts a helical structure after occupying its inhibitory position in the $\alpha_D\beta_D$-catalytic interface of its cognate F_1, equivalent to IF_1 (26, 33).

Here, we analyzed the rotary dynamics of the recombinant expressed PdF_1. Unexpectedly, PdF_1 rotation exhibits only three intervening pauses per revolution (separated by 120°), and no obvious substeps were resolved. ATP binding and ATP hydrolysis apparently occur at the same angular position, revealing a chemomechanical coupling mechanism unique among currently characterized F_1-ATPases (Fig. 1*C*). Furthermore, we directly show that Mg-ADP and the ζ-subunit partially and totally inhibit the rotation of PdF_1, respectively. Our results suggest that both entities exert a regulatory role in determining the latent hydrolytic activity of PdF_1F_o ATP synthase.

Results

Recombinant Expression of PdF_1. The protein expression of the recombinant PdF_1 complex in the *E. coli* system was investigated in the presence and absence of coexpressed Atp12p, the *P. denitrificans* homolog of ATPAF2, an assembly factor of mitochondrial F_1 (34). Native polyacrylamide gel electrophoresis (PAGE) of the cytoplasmic fractions of the recombinant cells showed that coexpression of Atp12p significantly enhanced the expression of the PdF_1 complex (*SI Appendix*, Fig. S1*A*), revealing that the Atp12 protein is essential for the efficient production and assembly of PdF_1. This is a demonstration of this chaperone functioning in the assembly of a bacterial F_1-ATPase.

Previous studies revealed the importance of ATPAF1 (*Atp11*) and ATPAF2 (*Atp12*) in the assembly of the eukaryotic F_1, which have been proposed to prevent the aggregation of the β- and α-subunits (35). The conservation of the *Atp12* gene in the alphaproteobacteria genome (36) and its role in the building of the *P. denitrificans* enzyme evince a high similarity in the assembly process of PdF_1 and mitochondrial F_1.

To examine the rotary dynamics of the Pd enzyme, the mutant "PdF_1 γCC" (a PdF_1-ATPase with the following modifications: βHis tag, γQ115C, and γD214C) was engineered. Purified PdF_1 γCC was biotinylated with sodium dodecyl sulfate (SDS)-PAGE and western blot analysis, revealing an appropriate subunit composition and the specific biotinylation of the γ-subunit (*Materials and Methods* and *SI Appendix*, Fig. S1 *B* and *C*).

ATP Hydrolysis of PdF_1 γCC. PdF_1 typically has tightly regulated ATP hydrolysis activity (27), which can be partially relieved by the removal of its intrinsic regulatory ζ-subunit or by the presence of either lauryldimethylamine oxide (LDAO) or oxyanions (28, 32). We quantified the hydrolytic activity of PdF_1 γCC in the absence of an activator. As expected, since our recombinant complex does not contain the inhibitory ζ-subunit, an ATPase-specific activity of $5.1 \pm 0.4\ s^{-1}$ (± SE; 0.85 units per milligram of protein) was observed, higher than that reported for PdF_1

purified from *P. denitrificans* cells (0.14 units per milligram of protein) but similar to the activity of pure F_1 obtained from a *P. denitrificans* ζ-knockout strain (PdΔζ; 0.87 units permilligram of protein) (37). Furthermore, the addition of 0.1% LDAO resulted in an 11-fold increase in activation, showing a specific activity of 56.7 ± 3.6 s^{-1} (± SE) (Fig. 2*B*), similar to but higher than the fivefold activation obtained with the $PdF_1^{\Delta\zeta}$ preparation when LDAO is included in the assay (37). Additionally, the reconstitution of the ζ-subunit led to a complete inhibition of PdF_1 γCC ATP hydrolytic activity, in agreement with previous studies (26, 32) (*SI Appendix*, Fig. S1*D*). Overall, these data corroborated the biochemical characteristics of PdF_1 γCC, confirming that the recombinant mutant possesses similar characteristics to the native PdF_1. For simplicity, PdF_1 γCC is referred to as PdF_1 hereafter.

Rotation Assay of PdF_1. PdF_1 was immobilized onto a nickel-nitrilotriacetic acid–coated glass via polyhistidine tags. The rotation was observed with a 40-nm gold nanoparticle attached to the γ-subunit as a probe (Fig. 2*A*). Images were taken with a high-speed camera at a recording speed of 10,000 frames per second (fps; 100 μs per frame). However, because PdF_1 possesses a latent ATP hydrolysis activity, almost no rotating particles were detected. Therefore, an ATPase activator (0.1% LDAO) and an ATP regeneration system were included in the reaction buffer. Under this condition, we easily observed CCW rotation of PdF_1 that was frequently interrupted by periods of rotation pause (likely caused by Mg-ADP inhibition; see below).

The overall speed of rotation, calculated from the lapses in continuous rotation, followed simple Michaelis–Menten kinetics with an apparent K_m for ATP of 78 ± 5 μM and V_{max} of 338 ± 6 (± SE) revolutions per second (rps) (Fig. 2*B*). Using these kinetic parameters, we estimated an apparent k_{on} for ATP of 1.3 × 10^7 M^{-1} s^{-1}, which was comparable with the k_{on} values of 3.0 × 10^7 and 2.7 × 10^7 M^{-1} s^{-1} for TF_1 and hMF_1, respectively (13, 21).

Interestingly, the maximum velocity obtained from single-molecule data (338 rps) mismatches that quantified by biochemical ATPase assay (ATPase/3 = 18.9 rps) (Fig. 2*B*). Previous evidence has shown a similar trend in the case of some F_1-ATPases, where these discrepancies have been attributed to Mg-ADP–mediated inhibition or to the selection of functional rotating enzymes in single-molecule experiments (21, 38, 39). Biochemical studies suggested that Mg-ADP regulates PdF_1-ATPase activity (40). Later, we explore the direct effect of Mg-ADP on PdF_1 rotary catalysis.

PdF_1-ATPase Exhibits Three-Step Rotation Regardless of the Concentration of ATP. The stepping behavior of PdF_1 was closely examined under low ATP concentration (<< K_m), middle ATP concentration (near K_m), and high ATP concentration (>> K_m). Previous single-molecule rotation studies revealed that, independent of their origin, all investigated F_1-ATPases display substeps in each 120° cycle (13, 15, 21, 22, 39, 41). For instance, TF_1, the archetypal bacterial F_1-ATPase for single-molecule studies, has two substeps, and hMF_1 has three substeps in each 120° cycle (Fig. 1 *A* and *B*). Since the dwell positions between steps at high and low ATP concentrations are generally different, substep behaviors are normally observed in F_1-ATPases at ATP concentrations near K_m. However, PdF_1 does not exhibit any

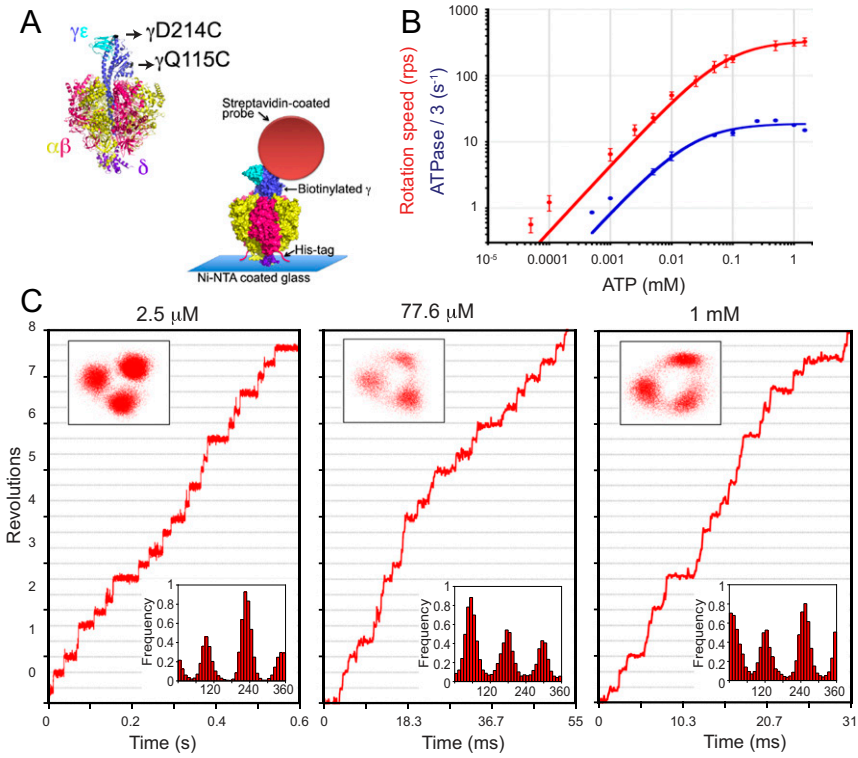

Fig. 2. ATP-driven rotation of PdF_1. (*A*) Single-molecule setup of PdF_1. Two cysteine residues of the rotor γ-subunit (black arrows) were used to attach the rotary probe using biotin-streptavidin, and His tag in the β-subunit was used to immobilize PdF_1 to the Ni-coated glass. (*B*) Time-averaged rotation speed of PdF_1 (red) and one-third of the bulk-phase ATPase rate (blue) vs. Mg-ATP concentration. Solid lines show Michaelis–Menten fits. V_{max} = 338 ± 6 rps and K_m = 77.6 ± 5.3 μM for rotation and V_{max} = 18.9 ± 1.2 s^{-1} and K_m = 22.1 ± 8.2 μM for ATPase/3. Error bars represent SD. (*C*) Time courses of three different rotating particles observed under different [ATP] (indicated at the top of each graph). *Upper Insets* and *Lower Insets* display *xy* trajectories of the centroids and angular distributions, respectively. For each particle, the reference angle was arbitrarily assigned. In *B*, three repetitions were done for each measurement of ATPase. In *B* and *C*, 20 rotating molecules were analyzed per condition in the single-molecule analysis. Ni-NTA, nickel-nitrilotriacetic acid.

substep, and only three intervening pauses (separated by 120°) at all [ATP] investigated were identified (Fig. 2*C*).

Statistical analysis of the intervals between steps under low [ATP] showed a single exponential decay function (Fig. 3 *A–C*). The rate constants determined from the dwell time histograms (τ_1) were proportional to [ATP], confirming these waiting times as the ATP binding dwells (Fig. 3*H*). The estimated rate constant for ATP binding (k_{on}) was 1.6 ± 0.3 (± SD) × 10^7 M^{-1} s^{-1}, in agreement with the k_{on} of 1.3 × 10^7 M^{-1} s^{-1} calculated from the Michaelis–Menten analysis.

At [ATP] near K_m (Fig. 3*D*) and under V_{max} conditions (Fig. 3 *E* and *F*), the histograms of dwell time between successive steps obeyed a two-consecutive reaction model. Two time constants were calculated in each condition, designated as τ_1' and τ_2 for the condition near K_m and τ_2 and τ_3 for conditions with saturated [ATP]. Time constants τ_2 and τ_3 were independent of [ATP] (Fig. 3*H*), supporting their association with ATP hydrolysis and product release events, while τ_1' appears to be the sum of the binding dwell and the catalytic dwell (likely τ_3). Overall, these results suggest that at least three elementary reactions occur at the same angular position, most likely ATP binding (τ_1), ATP hydrolysis, and product release (τ_2 and τ_3). However, the identities of the elementary steps that correspond to τ_2 and τ_3 remain unclear.

To confirm the absence of substepping behavior in the chemomechanical coupling reaction of PdF_1, we observed the rotation of PdF_1 in the presence of a slowly hydrolyzable ATP analog, ATPγS [adenosine-5′-O-(3-thiotriphosphate)], that allows a detailed analysis of the stepping rotation of F_1. The slowed ATPγS catalysis results from a deceleration of the hydrolytic reaction of TF_1 and bMF_1 (20, 42) and also, the release of a phosphate analog (thiophosphate) with the hMF_1 enzyme (21). ATPγS-driven rotation of PdF_1 obeyed a Michaelis–Menten model (*SI Appendix*, Fig. S2*A*), giving a K_m of 1.8 ± 0.3 μM and V_{max} of 5.9 ± 0.2 rps (± SE). V_{max} was 57-fold slower than its rotation with ATP (338 rps). As with ATP, PdF_1 exhibited only 120° steps at all [ATPγS] examined (*SI Appendix*, Fig. S2), supporting the absence of additional subpauses.

We analyzed the duration of the pauses displayed at different ATPγS concentrations. We observed that at low [ATPγS], the histogram of dwell time obeyed a single-reaction model, and one reaction constant was estimated (τ_1) (*SI Appendix*, Fig. S3*A*). At concentrations near K_m and saturated [ATPγS], histograms of dwell time followed a double exponential function (*SI Appendix*, Fig. S3 *B–F*).

The reaction constants estimated at saturated [ATPγS] (designated as τ_2 and τ_3) were independent of the substrate concentration (*SI Appendix*, Fig. S3 *E–G*), suggesting their association with the hydrolytic event or product release. Neither were similar to the reaction constants estimated at saturated ATP. Therefore, we suggest that ATPγS extended both the hydrolytic event and the product release event. However, the exact identity of the elementary step(s) associated with τ_2 and τ_3 remains unclear.

As expected, two reaction constants were estimated at concentrations around K_m, designated τ_1 and "$\tau_2 + \tau_3$" (*SI Appendix*, Fig. S3 *B–D*). The waiting times τ_1 were inversely proportional to [ATPγS], supporting the hypothesis that these are the binding

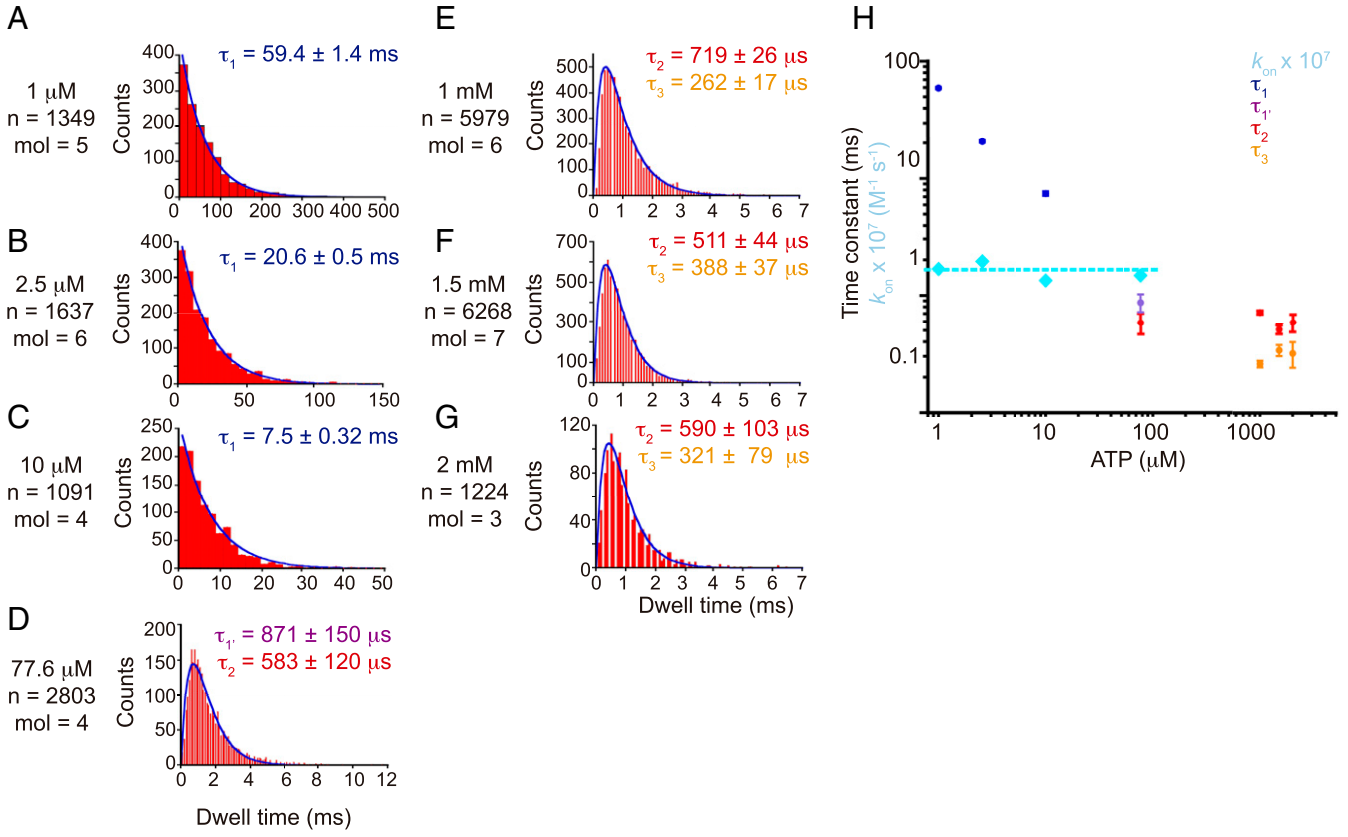

Fig. 3. Dwell distributions for a composite of PdF_1 molecules at different [ATP]. In each graph, τ denotes the time constant calculated from fitting (solid line) a single exponential decay function (*A–C*) or a double exponential decay function (*D–G*). At the left of each graph, [ATP], the total number of dwells summed (*n*), and the number of molecules collectively analyzed (mol) are displayed. (*H*) ATP concentration dependency of the time constants. The τ_1-constants were used to calculate the second-order rate constant of ATP binding (k_{on}), and the obtained values were plotted against ATP concentration in light blue squares. Error bars represent SE.

dwells (*SI Appendix*, Fig. S3*G*). The estimated k_{on} for ATPγS binding based on the values of τ_1 was 8.2 ± 2.6 (± SD) × 10^6 M^{-1} s^{-1}, in agreement with the k_{on} of 9.8 × 10^6 M^{-1} s^{-1} calculated from $3 \times V_{max}/K_m$, confirming that τ_1 represents the binding rate. On the other hand, the waiting times "$\tau_2 + \tau_3$" were independent of the substrate concentration and appeared to be the sum of $\tau_2 + \tau_3$ (*SI Appendix*, Fig. S3*G*). Overall, our results reinforce the notion that substrate binding and two other substrate-independent elementary steps occur at the primary dwells, the most likely candidates being the hydrolytic reaction and product release.

Binding and Catalytic Dwell Share the Same Angular Position in PdF_1. The absence of any substepping behavior in the rotary mechanism of PdF_1 suggests that the elemental reactions may occur in the same angular position. To test this hypothesis, we compared the dwell positions of single PdF_1 molecules at low ATP concentration (ATP binding dwells) and those at high ATP concentration (catalytic pauses).

The increase in the rotation speed from 14.1 ± 2.9 rps (at 2.5 μM ATP) to 343 ± 61 rps (± SD; at 1 mM ATP) after buffer exchange confirmed the increase in [ATP] (Fig. 4*A*). Examination of the bead centroid revealed three discrete 120° pauses under both conditions (Fig. 4 *B* and *C*). The difference in dwell angles (Δθ) after increasing [ATP] was only 0.5° ± 0.3° (± SE), suggesting the catalytic pause of PdF_1 occurs at the same angular position of the ATP waiting pause (Fig. 4*D*).

For further confirmation, we identified the angular position of ATP hydrolysis using the nonhydrolyzable ATP analog 5′-adenylyl-imidodiphosphate (AMP-PNP) (43) and compared its inhibitory stall with the ATP binding events. For this, we used a 200-nm magnetic bead duplex as a probe in place of a 40-nm gold nanoparticle to give us a manipulatable "handle" on PdF_1.

First, we observed the stepping rotation of a PdF_1 molecule under substrate-limiting conditions (0.5 μM ATP << K_m = 4.1 ± 0.5 μM [± SE]) (*SI Appendix*, Fig. S4). Following this, a buffer containing 0.5 μM AMP-PNP was gently introduced into the flow chamber with 0.5 μM ATP. After the infusion of AMP-PNP, the particles continued rotating for 1 to 2 min before they stopped and did not spontaneously resume rotation through the end of the experiment (Fig. 5*A*). The AMP-PNP–inhibited state did not resume active rotation even if forcibly rotated with magnetic tweezers. This allows for the discrimination of AMP-PNP inhibition from the ADP-inhibited form that is readily reactivated with magnetic tweezers (44). The angular distance (Δθ) of the AMP-PNP inhibitory state from the nearest binding angle revealed a mean difference of −5.5 ± 0.5° (± SE) (Fig. 5 *B* and *C*), supporting the finding that the ATP binding and ATP cleavage dwells share nearly the same angular position.

Overall, these results suggest that the rotary behavior of PdF_1 is different from other F_1's. However, 0.1% LDAO was added to the reaction buffer in all experiments as an ATPase activator (45–47). Although single-molecule studies on other F_1's show that LDAO extends the duration of the actively rotating state and shortens the duration of the inhibitory pausing state without

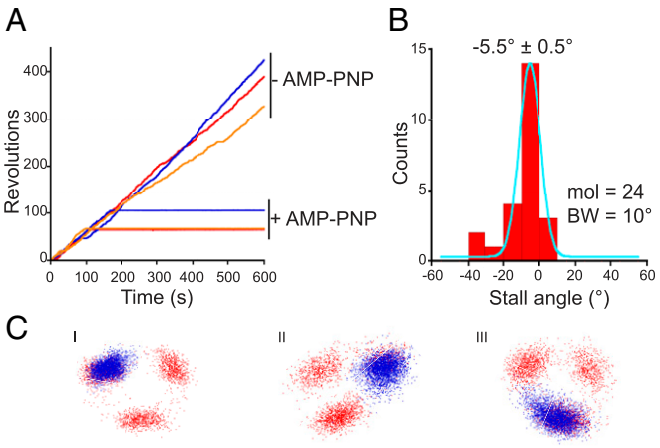

Fig. 5. Identification of the catalytic dwell by AMP-PNP. (*A*) Rotation of three PdF_1 molecules (red, blue, and orange) before and after the addition of 0.5 μM AMP-PNP in the presence of 0.5 μM ATP. A submicrometer magnetic bead was used, and recordings were taken at 60 fps at 25 °C. (*B*) Angle distribution of AMP-PNP–induced stalls relative to the nearest ATP binding dwell. The solid line represents the fit to a Gaussian equation. The mean value (± SE) is displayed. BW, bin width; mol, molecules analyzed. (*C*) Stall positions of the AMP-PNP–inhibited state (blue) are superimposed on the *xy* trajectories (red) that show the positions of the ATP binding dwells (three representative particles are displayed).

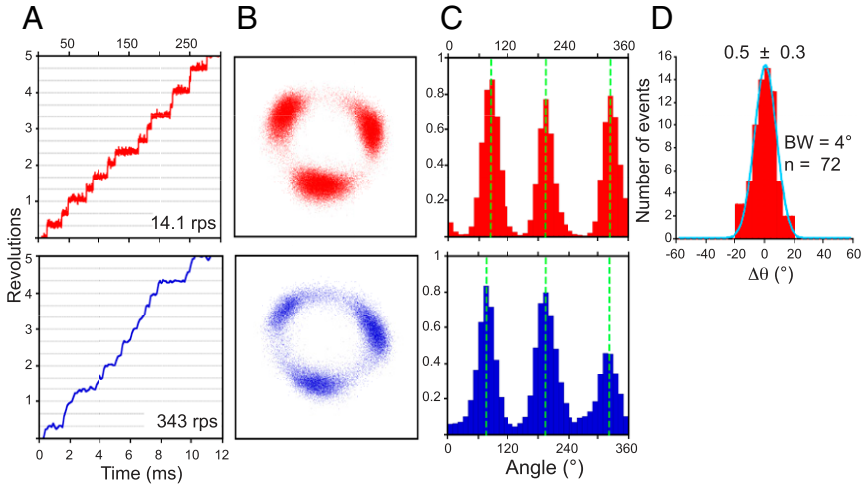

Fig. 4. Observation of a single rotating PdF_1 under low (red) and high (blue) [ATP]. One representative particle, from 24 molecules analyzed, is displayed. (*A*) Time courses of the rotation (rotation speed). (*B*) The *xy* position of the bead centroid. (*C*) Histograms of the angular position. The dashed lines highlight the mean value obtained from fitting a Gaussian distribution. (*D*) Distribution of the angular difference between the position of ATP cleavage relative to ATP binding (Δθ). The solid line represents the fit to a Gaussian model, and the value of the mean difference (± SE) is shown. For this experiment, 40-nm gold particles and a recording rate of 10,000 fps were used. BW, bin width; *n*, number of events analyzed.

affecting the principle rotation mechanism (38, 39), we analyzed the rotation of single particles in the presence and absence of the detergent (under low and saturated ATP concentrations) for confirmation that the PdF_1 rotary mechanism is not affected by LDAO (*SI Appendix*, Fig. S5). At both ATP concentrations, we observed that LDAO reduces both the rotation velocity of PdF_1 and the duration of the inactive state (likely the ADP-inhibited state) (*SI Appendix*, Fig. S5 *A* and *D*). We believe the sum of both effects resulted in the activation observed in bulk assays of PdF_1 (where an ensemble of molecules is analyzed). Most importantly, we compared the angular position of the ATP binding (at low ATP concentration) and hydrolytic dwells (at saturated ATP) in the presence and absence of LDAO. The angular distance ($\Delta\theta$) before and after including 0.1% LDAO was only $-5.7° \pm 0.4°$ ($\pm$ SE) for limiting [ATP] (*SI Appendix*, Fig. S5 *B* and *C*) and $-2.0° \pm 0.4°$ ($\pm$ SE) for high [ATP] (*SI Appendix*, Fig. S5 *E* and *F*), confirming that LDAO did not alter the angular position of the elementary dwells and suggesting that our results are consistent with the rotary mechanism in the absence of activators.

P_i Release. Our experimental results indicated that in the rotary mechanism of PdF_1, binding and catalytic events occurred at the main dwells. The absence of any additional pauses in the PdF_1 rotation (aside from the primary dwells) and the estimation of three time constants in the main pauses (derived from the dwell time analysis) suggested that ADP/P_i release events also occur at the same angular position. We analyzed the effect of a large amount of P_i on PdF_1 rotation to identify the angular position of the product release events.

Previous studies revealed that the addition of high P_i concentrations decelerates TF_1 rotation rate as a consequence of extension of the dwell associated with waiting for P_i release (14). As observed in *SI Appendix*, Fig. S6, the speed of PdF_1 rotation, driven by 1 mM ATP, decreased as [P_i] increased, leading to a ~95% decrease in velocity at 300 mM P_i (*SI Appendix*, Fig. S6*A*). However, PdF_1 still showed three-stepping rotation without obvious substeps. Backward steps were also not observed at any [P_i] tested (*SI Appendix*, Fig. S6*B*). These results suggest that PdF_1 is a principally three-stepping motor. However, it should be noted that the suppression effect of P_i is not only by product inhibition but also, by high ionic strength, considering that 500 mM KCl or 200 mM K_2SO_4 with comparable ionic strength to that of 300 mM P_i also suppressed the rotation velocity at similar levels (*SI Appendix*, Fig. S6*C*).

PdF_1 Torque Is Similar to That Estimated for TF_1. Previously, McMillan et al. (39) suggested that a high torque may be a characteristic of unidirectional F_1F_o ATP synthases, as single-molecule studies of *Caldalkalibacillus thermarum* strain TA2.A1 F_1-ATPase ($TA2F_1$) revealed. To examine whether PdF_1 shares this characteristic, we determined its torque using a 200-nm magnetic bead duplex as a probe and analyzed the fluctuating behavior of its rotational angle (θ) by employing fluctuation theorem (FT) analysis. FT analysis has been widely used to estimate the driving power of motor proteins based on fluctuations in their motion without the need for an accurate measurement of a frictional drag coefficient or the application of external stall torque (48). FT analysis of 15 PdF_1 rotation traces under saturating ATP (2 mM) revealed a rotary torque of 33.8 ± 5.4 piconewton nanometers (pNnm), similar to the torque generated by TF_1 under the same experimental conditions (34 ± 5.4 pNnm) (*SI Appendix*, Fig. S7) and to the torque previously reported for TF_1 (35 ± 2.8 pNnm; $\pm$ SD) (48). This analysis suggests that torque may only be an influence in totally unidirectional F_1 such as $TA2F_1$ (49) and that motors with latent ATP hydrolysis, such as PdF_1, are not as influenced in this way, suggesting that there is another reason for minimal ATP hydrolysis.

Pause and Stall of PdF_1 Rotation by Inhibitors. The mechanisms involved in the tight inhibition of PdF_1 hydrolytic activity have been intensely studied. Two primary regulatory mechanisms have been proposed: Mg-ADP inhibition (40) and ζ-inhibition (30, 32). To determine whether the Mg-ADP inhibitory mechanism is conserved in the Pd enzyme, we observed the rotation of PdF_1 in the presence of 1 μM ADP and 1 μM ATP and the absence of an ADP-trapping system (Fig. 6*A*). Under these conditions, the continuous rotation of PdF_1 was frequently interrupted for pauses too long to be attributed to the ATP waiting dwell (240 ± 12 ms; $\pm$ SE) (Fig. 6*B*). Rotation spontaneously restarted after 21.3 ± 0.5 s ($\pm$ SE) (Fig. 6*C*). The removal of free ADP by infusion of a buffer containing an ADP-trapping system into the flow chamber decreased the length and frequency of the long pauses (11.8 ± 0.9 s; $\pm$ SE) (Fig. 6 *A* and *C*), supporting the conclusion that they are a result of Mg-ADP inhibition.

Next, we investigated the effect of the ζ-subunit on PdF_1 rotation. We compared the rotation of single particles under limiting ATP concentration (0.5 μM) before and after the addition of 5 μM *P. denitrificans* ζ-subunit (Pdζ) (Fig. 6*E*). The addition of Pdζ stalled the rotation of PdF_1, likely forming a stable ζ-inhibited state from which the enzyme did not spontaneously escape within the 10-min observation period.

We also examined whether PdF_1 molecules in Mg-ADP inhibition or ζ-inhibition can be reactivated with forcible rotation in the CCW direction using magnetic tweezers, as reported for ADP-inhibited TF_1 (44). Pausing PdF_1 was rotated for two revolutions in the CCW direction at 1 rps and released from the magnetic tweezers. In the case of ADP-inhibited PdF_1, most of molecules resumed rotation (83.3%; $n = 12$). In contrast, none of the ζ-inhibited molecules observed resumed rotation ($n = 13$), revealing an intrinsic difference in the stability and mechanism of both forms of hydrolytic inhibition.

Overall, our results confirmed that the Mg-ADP inhibitory mechanism is conserved in PdF_1 and revealed that the regulatory mechanism of the ζ-subunit on PdF_1 is similar to the one exerted by IF_1 on hMF_1 (21). In addition, we determined the angular position of the Mg-ADP and ζ-inhibitory states relative to the location of the ATP binding state. The statistical analysis revealed that both inhibitors stop the rotation at an angular position identical to that of the ATP waiting state (Fig. 6 *D* and *F*). Previous studies reported that Mg-ADP stops the rotation of the bacterial TF_1 enzyme at the catalytic dwell (38), similar to the effect of Mg-ADP and IF_1 on the rotation of the eukaryotic hMF_1 (21). Collectively, these data suggest that Mg-ADP and the ζ-subunit lock the PdF_1 enzyme in the precatalytic step. The small angular difference between the inhibitory states and the ATP binding dwell indicates that the binding and catalytic dwells share the same angular position in PdF_1.

Discussion

We characterized the stepping rotation of *P. denitrificans* F_1-ATPase. The PdF_1 rotates γ-subunit unidirectionally in a CCW direction, exhibiting only three main pauses separated by 120° at all ATP and ATPγS concentrations tested, above or below K_m. Three different time constants in the main pauses were obtained from analysis of dwell times, suggesting that at least two reactions other than ATP binding limit the primary dwell (likely ATP cleavage and ADP/P_i release). Furthermore, no substeps were detected in PdF_1 under all of the conditions tested, in contrast to all other investigated F_1's that show substepping behaviors when their rotation is characterized by single-molecule studies (13, 15, 21–23, 39, 41).

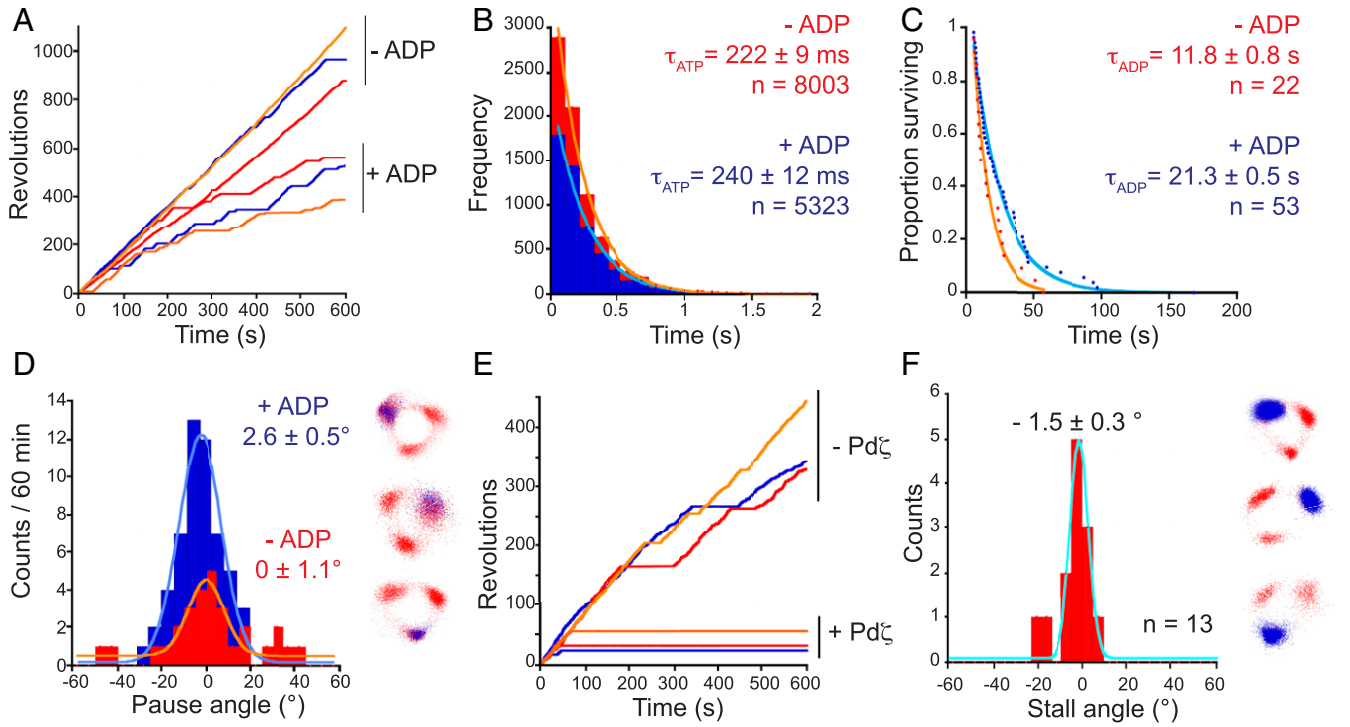

Fig. 6. PdF_1 inhibitory states. PdF_1 rotation was observed in the presence of limiting [ATP] and the components indicated below. (*A*) Rotation of three particles (red, blue, and orange) in the presence or absence of 1 μM ADP. Ten molecules were analyzed in total. (*B*) Dwell time analysis of the ATP binding process. Dwells shorter than 5 s were collected and collectively analyzed. (*C*) Decay in the number of pausing F_1-ATPases in the presence (blue) or absence (red) of ADP. (*D*) Pausing position of the Mg-ADP–inhibited state. (*E*) Rotation of three particles (red, blue, and orange) before and after the addition of 5 μM Pdζ. (*F*) Stalling position induced by Pdζ. In *B* and *C*, solid lines show fits to single exponential functions, and time constants (± SE) are indicated. *D*, *Left* and *F*, *Left* display the angle distributions of the inhibitory states relative to the nearest ATP binding dwell. Solid lines represent fits to a Gaussian model, and the mean angular position (± SE) is indicated. In *D*, *Right* and *F*, *Right*, inhibitory states (blue) are superimposed on the *xy* trajectories (red) that show the ATP binding pauses (three particles are displayed). *n*, number of events analyzed.

The identification of ATP binding and ATP-hydrolytic dwells in single molecules revealed that both elementary steps occur at almost the same angular position in PdF_1-ATPase. This result was consistent with the inhibition experiments with AMP-PNP, Mg-ADP, and the ζ-subunit, which halted PdF_1 rotation at −5.5°, 2.6°, and −1.5° from the binding dwell, respectively. To date, most F_1's characterized using single-molecule techniques have shown that AMP-PNP inhibition and Mg-ADP inhibition stop rotation at the catalytic angle (21, 38), similar to the inhibitory stall of IF_1 on the rotation of hMF_1 (21), supporting the case for the absence of additional substeps in PdF_1 chemomechanical coupling.

Our present results suggest that at least one event in addition to ATP binding and ATP hydrolysis occurs at the position of the main dwell in PdF_1, likely phosphate or ADP release (or both combined). Nevertheless, the exact ADP/P_i release position in PdF_1 has not been directly identified. Previous studies have determined that the bacterial TF_1 conducts P_i release at the same angular position of the catalytic dwell (14); meanwhile, the eukaryotic enzyme hMF_1 performs P_i release at a new dwell at +65° after the binding dwell (21). In the bacterial TF_1, ADP release has been established at the position of the ATP binding dwell (14). An interesting finding in EF_1 observed that elevated [ADP] slows its rotation at −30° before the catalytic dwell (23), suggesting that it has a different ADP release position than TF_1.

Here, we observed that the addition of elevated concentrations of P_i (*SI Appendix*, Fig. S6) or ADP (*SI Appendix*, Fig. S8) to PdF_1 did not expose any new dwell during its ATP-driven rotation. Neither did it extend the duration of a particular dwell in a specific manner. Therefore, the exact P_i release and ADP release position in PdF_1 requires further investigation. These results suggest that the affinity of P_i and ADP for the catalytic site after ATP hydrolysis is low. However, in the case of ADP, we observed a dramatic reduction in the number of rotary molecules (likely caused by their arrest during the ADP inhibitory state), suggesting that ADP binding at the inhibitory position is more favorable.

Based on our results, we propose a reaction scheme for PdF_1 (Fig. 1*C*) that is strikingly similar to the rotary binding change mechanism proposed by Boyer (50), Mitchell (51), and Duncan et al. (52) and later modified by Weber and Senior (53) and Adachi et al. (14) to amend the occupancy of the catalytic sites to alternate between two and three sites. In our model, three intervening dwells compose one revolution. Any given dwell comprises ATP binding dwell, catalytic dwell, and likely product (or products) release dwell. However, the chronological order of product dissociation has not yet been directly resolved (indicated with dashed arrows in Fig. 1*C*). A list of possible models, although not exhaustive, is displayed (*SI Appendix*, Fig. S9).

It is important to emphasize that although all our experimental results show the absence of any apparent substepping behaviors in PdF_1 rotation and imply that all catalytic events in PdF_1 occur at the primary dwell position, further experiments are necessary to establish the exact position of product release. Nevertheless, the coincidence of angles for ATP binding and catalysis is distinctive from what is observed in all other characterized F_1-ATPases. Furthermore, under all of the conditions presented here, there is no evidence of new subpauses associated with the ADP/P_i release dwell. It is safe to conclude that the PdF_1 chemomechanical scheme is different from the schemes of all other known bacterial or eukaryotic F_1-ATPases.

The exact elementary steps that trigger PdF_1 γ-rotation remain elusive. However, we suggest ATP binding as the primary

Table 1. Stepping pattern of PdF_1F_o and other rotary ATPases

Protein	Protein thermostability	Domain of life	Physiological function	Proteolipid/ring	Dwell/turn in F_1/V_1	Source
TF_1F_o	Thermophile	Bacteria	ATP synthase/hydrolase	10*	$6^{\dagger,\ddagger}$	(13, 66)
EF_1F_o	Mesophile	Bacteria	ATP synthase/hydrolase	10*	$6^{\dagger,\S}$	(15, 67)
hMF_1F_o	Mesophile	Eukarya	ATP synthase	$8^{\P}$	$9^{\dagger,\ddagger}$	(21, 65)
bMF_1F_o	Mesophile	Eukarya	ATP synthase	$8^{\#}$	$9^{\dagger,\ddagger}$	(20, 65)
YMF_1F_o	Mesophile	Eukarya	ATP synthase	$10^{\#}$	$6^{\dagger,\S}$	(6, 22)
PdF_1F_o	Mesophile	Bacteria	ATP synthase	$12^{\#}$	$3^{\dagger,\ddagger}$	(33); this study
TtV_1V_o**	Thermophile	Bacteria	ATP synthase	12*	$3^{\dagger,\ddagger}$	(62, 68)
$EhV_1V_o^{\dagger\dagger}$	Mesophile	Bacteria	ATP hydrolase	$10^{\#}$	$6^{\dagger,\ddagger}$	(63, 69)

*Values confirmed by electron cryomicroscopy analysis.
†Values determined by single-molecule analysis using gold nanoparticles as a rotary probe.
‡Forty-nanometer gold nanoparticles were used.
§Sixty-nanometer gold nanoparticles were used.
¶Values suggested according to phylogenetic analysis.
#Values confirmed by crystallography.
**Tt (*Thermus thermophilus*).
††Eh (*Enterococcus hirae*).

torque-generating step, consistent with the rotary mechanism of other F_1-ATPases (23, 54–56), although there remains the possibility that another reaction step is responsible for torque generation. Due to the unique rotary scheme of PdF_1, the exact position and order of product releasing steps remain uncertain in this enzyme. Currently, the only resolved crystallographic structure of PdF_1 is in the ζ-inhibitory state (Protein Data Bank ID code 5DN6) (33), in which the rotation is likely hindered in the catalytic dwell. In this structure, one catalytic site is empty, and the remaining catalytic sites hold Mg-ATP. If we assume that this crystal structure represents a catalytic intermediate state, the nucleotide occupancy of this crystal would suggest that the release of the products from the previous intermediate state with full occupation (one catalytic site occupied by one or both products and the remaining sites holding Mg-ATP) occurs before the hydrolysis of ATP (*SI Appendix*, Fig. S9). However, other models should not be rejected. High-resolution structural analysis and further stall and release experiments could elucidate the fine details of the chemomechanical scheme of PdF_1.

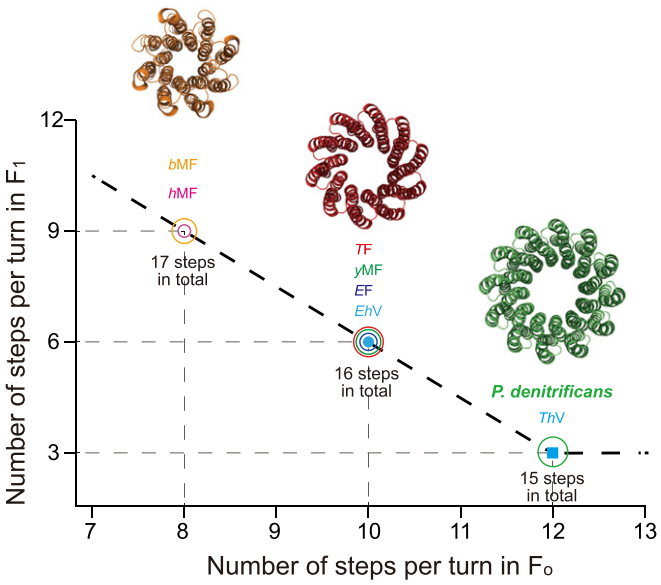

Fig. 7. Comparison of number of proteolipid subunits per ring vs. the number of steps/turn in the rotary scheme of F_1- and V_1-ATPases. Shown is a comparison of TF (*Bacillus PS3*), EF (*E. coli*), *h*MF (human mitochondria), *b*MF (bovine mitochondria), *Y*MF (*S. cerevisiae*), PdF (*P. denitrificans*), TtV (*Thermus thermophilus*), and EhV (*Enterococcus hirae*). Structures of the c8 ring of bMF_o (orange), c10 ring of TF_o (red), and c12 ring of PdF_o (lime green) are shown. Details and appropriate references are in Table 1.

Two main differences between the rotary scheme of PdF_1 and other F_1's were observed: 1) the angular difference between the binding and catalytic dwells and 2) the total number of dwells per revolution. To date, all characterized F_1's conduct ATP binding and ATP cleavage in two different dwells (at 80° to 90° apart from each other) and display six (TF_1, EF_1, and YMF_1) (13, 15, 22) or nine (bMF_1 and hMF_1) (20, 21) pauses per turn, depending on the presence of an additional dwell, likely associated with P_i release (21). Although it is interesting to note that advanced statistical analysis suggests that TF_1 makes small substeps during catalytic dwell, this has not been resolved experimentally or by conventional analysis methods (57). On the other hand, PdF_1 conducts ATP cleavage and ATP binding almost at the same dwell, and only three intervening pauses per turn could be identified.

We tentatively propose that variations in the F_1 rotary schemes could be attributable to discrete differences between their overall structures. The γ-subunit is the most plausible candidate for this structural diversity, given that Pd-γ has lower amino acid conservation than Pd-α and Pd-β compared with their mitochondrial and bacterial counterparts (*SI Appendix*, Table S1). Coincidentally, in silico modeling showed that the alteration of specific portions of the γ-subunit could affect the energetic barriers that define the stepped rotary pattern of the bMF_1 enzyme (58).

Interestingly, a similar rotary scheme, where ATP cleavage and ATP binding occur at nearly the same angle, has been observed in various vacuolar ATPases (V_1-ATPases) and archaeal ATPases (A_1-ATPases) (59–61), a group of molecular motors distantly related to F_1-ATPase that conserve a similar holostructure and rotary mechanism. Analogous to the F_1-ATPases, V_1- and A_1-ATPases exhibit a variety of stepping behaviors, and rotary schemes with three (62) and six pauses/turn (63) have been identified. Previous studies have tried to discern the features of the ATPase machinery that could determine the stepping behavior of their rotary schemes. However, results indicate that characteristics such as thermostability, phylogenetic domain, or physiological function could not uniquely define the pattern of catalytic dwell angles (Table 1).

Here, we observed an inverse correlation between the number of steps in the rotary scheme of F_1/V_1 and the number of proteolipids per oligomer ring in their respective ion-conducting motors (F_o/V_o) (Fig. 7) (64). Thus, we propose that this feature could be related to the evolutionary adaptation of the chemomechanical coupling. Structural studies have suggested different copy

numbers of proteolipids (n) in the F_o/V_o ring, depending on the organism they come from (6, 33, 65–69). The "n" value matches the number of ions transported per turn of the F_o/V_o ring (when each proteolipid possesses one binding site for one coupling ion) and has been related to the stepping pattern of the rotary ring (4, 62).

Notably, in all of the enzymes we analyzed, ATPases with more steps co-occur with ion-conducting motors with fewer steps, resulting in a total number of steps that varies from 15 to 17 (Fig. 7). We believe these values could be related to the designed potential minima that govern the ATPase machinery. This could derive from symmetry or asymmetry between n and the three catalytic subunits in F_1/V_1. However, due to limited information, only F/V ATP synthases with ring stoichiometries of 8, 10, or 12 were analyzed. It would be interesting to investigate the stepping behavior of ATPases coupled with F_o/V_o rings with different numbers of proteolipids (70–73), considering that a minimum of three steps in the F_1/V_1 portion should be maintained according to total conservation of the threefold symmetry of this portion. Further studies will elucidate whether this correlation reflects a selection pressure that determines the stepping action of F_1- and V_1-ATPases and if this trend could reveal a common design principle of the rotary ATPase family.

Finally, we explored the features that define the latency of the PdF_1F_o complex in the hydrolysis of ATP. A previous study suggested that the differences in torque across species may be related to their resistance to rotation in the hydrolytic direction (39). The torque of PdF_1 (33.8 pNnm) did not fully reflect the lack of ATP hydrolysis that characterized the PdF_1 complex and is very similar to the one estimated for hydrolytically active TF_1 (34 pNnm). This result suggests that, at least in the case of PdF_1, the overall structure determines the basic properties of its rotary dynamics, with the main influence on physiological function derived from regulatory mechanisms.

Currently, there is an ongoing discussion to determine if the ζ-subunit or Mg-ADP has the dominant influence in the latent hydrolysis of PdF_1F_o. Recently, two *P. denitrificans* mutants lacking the ζ-subunit gene were studied. One ζ-knockout causes a specific growth defect associated with the activation of the ATP hydrolytic activity of PdF_1F_o (37). However, the other knockout caused only a moderate increase in PdF_1F_o ATP hydrolysis, which is insufficient to activate the membrane ATPase (74). We have previously hypothesized which differences in the strains could explain these apparent discrepancies (75).

In this study, we confirmed that Mg-ADP and the ζ-subunit tightly regulate PdF_1-ATPase activity. However, we observed stark differences in the mean lifetime of their inhibitory states and their tendency to reactivate ATP hydrolysis from an inactive state. While Mg-ADP inhibition has a mean duration of ∼30 s and its inhibitory action is spontaneously relieved, the ζ-subunit–mediated inhibition period is extended for more than 500 s and is not spontaneously relieved. These differences suggest that Mg-ADP only modulates PdF_1-ATPase activity, whereas the ζ-subunit completely blocks the rotation of the enzyme in the hydrolytic direction. Overall, our results support the ζ-subunit acting as a total inhibitor of PdF_1 ATP hydrolysis (in vitro) and are in accordance with a critical role of ζ as a physiological PdF_1F_o-ATPase inhibitor as described by Mendoza-Hoffmann et al. (37).

In summary, our results indicate that the reaction scheme of PdF_1 is likely different from that of other bacterial and eukaryotic F_1-ATPases, despite its high conservation with its mitochondrial counterpart. This finding suggests that subtle differences (in the structure or sequence) can heavily influence the rotary mechanism of F_1. Additionally, substepping behaviors are not a prerequisite for successful rotation and torque production in F_1-ATPase. Whether the simplified rotary mechanism of PdF_1 is conserved in other F_1's of the alphaproteobacteria class remains unknown. However, since substantial evidence supports alphaproteobacteria being closely related to the proto-endosymbiont from which mitochondria emerged (25), we believe that future comparative and phylogenetic analyses could provide interesting information regarding the evolution of the mitochondrial F_1 rotary mechanism. How individual species deal with different rotary schemes and the advantage any of these may confer now require further study.

Materials and Methods

Preparation of PdF_1. The F_1 operon (atpHAGDC) and the gene of the chaperone Atp12p were amplified from *P. denitrificans* genomic DNA. The genes for α-, γ-, β-, δ-, and ε-subunits (with a 10-histidine tag at the N terminus of the β-subunit) were introduced into the expression plasmid pTR19v43 to generate the plasmid "$pPdF_1$ WT." The atp12 gene was introduced at the end of the PdF_1 operon to generate the plasmid "$pPdF_1$ WT (+ atp12)." In addition, Q115 and D214 residues of the γ-subunit were substituted to cysteine using a site-directed mutagenesis method, generating the plasmid "$pPdF_1\gamma$CC (+ atp12)." All of the resulting plasmids were individually transformed into an F_1F_o-deficient *E. coli* strain, DK8 (76). Finally, all of the mutant preparations were confirmed by DNA sequencing.

Protein Purification. PdF1 was expressed and purified as described previously (21, 39), with some minor modifications (procedure is described in detail in *SI Appendix*). The purification was performed at room temperature, and the purified F_1 was stored at −80 °C until further use.

Single-Molecule Rotation Assays. The PdF_1 rotation assay was performed as described previously using either a ∼0.2-μm magnetic bead duplex or a 40-nm gold nanoparticle (44, 48, 77). The detailed procedures are described in *SI Appendix*.

Torque Measurements. The continuous torque (newtons) of PdF_1 and TF_1 was estimated from the rotation trajectories at 2 mM ATP using magnetic duplex beads, based on FT analysis (48). It was calculated using the equation $n = (k_BT/\Delta\theta) \bullet \ln[P(\Delta\theta/P(-\Delta\theta)]$, where k_BT denotes the thermal energy and $P(\Delta\theta)$ denotes the probability density of the distance traveled within a given time. Only enzymes exhibiting clear continuous rotation and angular velocity (nearly constant for at least 5 s) were selected for the analysis. The torque of each molecule was defined as the maximum value obtained via the FT analysis when employing a 5-s moving window, with windows starting at 1-ms intervals.

Other Procedures. The Pdζ-subunit was purified as described previously (30). PdF_1-ATPase activity was monitored by enzyme-coupled pyruvate kinase/lactate dehydrogenase ATPase assays as described elsewhere.

Data Availability. All data are available in the text or *SI Appendix*.

ACKNOWLEDGMENTS. We thank Dr. R. Watanabe for critical discussion, Dr. Y. Minagawa for his help with the data acquisition software, and all members of the laboratory of H.N. for valuable comments. This work was supported in part by National Council of Science and Technology of Mexico Fund I0010 Fellowship 277592 (to M.Z.-Z.), by National Autonomous University of Mexico Grants IN-221216 (to J.J.G.-T.) and IN-217520 (to J.J.G.-T.) from the General Direction of Academic Affairs–program for the support of research and technological innovation projects, and by Japan Society for the Promotion of Science Grant 17H06355 (to H.N.).

1. P. Mitchell, Coupling of phosphorylation to electron and hydrogen transfer by a chemi-osmotic type of mechanism. *Nature* **191**, 144–148 (1961).
2. V. Leone, D. Pogoryelov, T. Meier, J. D. Faraldo-Gómez, On the principle of ion selectivity in Na^+/H^+-coupled membrane proteins: Experimental and theoretical studies of an ATP synthase rotor. *Proc. Natl. Acad. Sci. U.S.A.* **112**, E1057–E1066 (2015).
3. D. Pogoryelov *et al.*, Microscopic rotary mechanism of ion translocation in the F_o complex of ATP synthases. *Nat. Chem. Biol.* **6**, 891–899 (2010).
4. M. G. Düser *et al.*, 36 degrees step size of proton-driven c-ring rotation in F_oF_1-ATP synthase. *EMBO J.* **28**, 2689–2696 (2009).
5. D. G. G. McMillan *et al.*, A_1A_o-ATP synthase of *Methanobrevibacter ruminantium* couples sodium ions for ATP synthesis under physiological conditions. *J. Biol. Chem.* **286**, 39882–39892 (2011).
6. D. Stock, A. G. Leslie, J. E. Walker, Molecular architecture of the rotary motor in ATP synthase. *Science* **286**, 1700–1705 (1999).

7. E. P. Gogol, E. Johnston, R. Aggeler, R. A. Capaldi, Ligand-dependent structural variations in *Escherichia coli* F_1 ATPase revealed by cryoelectron microscopy. *Proc. Natl. Acad. Sci. U.S.A.* **87**, 9585–9589 (1990).
8. J. P. Abrahams, A. G. Leslie, R. Lutter, J. E. Walker, Structure at 2.8 A resolution of F_1-ATPase from bovine heart mitochondria. *Nature* **370**, 621–628 (1994).
9. H. Noji, H. Ueno, D. G. G. McMillan, Catalytic robustness and torque generation of the F_1-ATPase. *Biophys. Rev.* **9**, 103–118 (2017).
10. H. Noji, R. Yasuda, M. Yoshida, K. Kinosita, Direct observation of the rotation of F_1-ATPase. *Nature* **386**, 299–302 (1997).
11. T. Ariga, E. Muneyuki, M. Yoshida, F_1-ATPase rotates by an asymmetric, sequential mechanism using all three catalytic subunits. *Nat. Struct. Mol. Biol.* **14**, 841–846 (2007).
12. R. Yasuda, H. Noji, K. Kinosita, M. Yoshida, F_1-ATPase is a highly efficient molecular motor that rotates with discrete 120 degree steps. *Cell* **93**, 1117–1124 (1998).
13. R. Yasuda, H. Noji, M. Yoshida, K. Kinosita, H. Itoh, Resolution of distinct rotational substeps by submillisecond kinetic analysis of F_1-ATPase. *Nature* **410**, 898–904 (2001).
14. K. Adachi *et al*., Coupling of rotation and catalysis in F_1-ATPase revealed by single-molecule imaging and manipulation. *Cell* **130**, 309–321 (2007).
15. T. Bilyard *et al*., High-resolution single-molecule characterization of the enzymatic states in *Escherichia coli* F_1-ATPase. *Philos. Trans. R. Soc. Lond. B Biol. Sci.* **368**, 20120023 (2013).
16. H. Noji *et al*., Rotation of *Escherichia coli* F_1-ATPase. *Biochem. Biophys. Res. Commun.* **260**, 597–599 (1999).
17. D. Spetzler *et al*., Single molecule measurements of F_1-ATPase reveal an interdependence between the power stroke and the dwell duration. *Biochemistry* **48**, 7979–7985 (2009).
18. H. Omote *et al*., The γ-subunit rotation and torque generation in F_1-ATPase from wild-type or uncoupled mutant *Escherichia coli*. *Proc. Natl. Acad. Sci. U.S.A.* **96**, 7780–7784 (1999).
19. D. Spetzler *et al*., Microsecond time scale rotation measurements of single F_1-ATPase molecules. *Biochemistry* **45**, 3117–3124 (2006).
20. R. Kobayashi, H. Ueno, C.-B. B. Li, H. Noji, Rotary catalysis of bovine mitochondrial F_1-ATPase studied by single-molecule experiments. *Proc. Natl. Acad. Sci. U.S.A.* **117**, 1447–1456 (2020).
21. T. Suzuki, K. Tanaka, C. Wakabayashi, E.-i. Saita, M. Yoshida, Chemomechanical coupling of human mitochondrial F_1-ATPase motor. *Nat. Chem. Biol.* **10**, 930–936 (2014).
22. B. C. Steel *et al*., Comparison between single-molecule and X-ray crystallography data on yeast F_1-ATPase. *Sci. Rep.* **5**, 8773 (2015).
23. J. Martin, R. Ishmukhametov, T. Hornung, Z. Ahmad, W. Frasch, Anatomy of F_1-ATPase powered rotation. *Proc. Natl. Acad. Sci. U.S.A.* **111**, 3715–3720 (2014).
24. J. V. Bason, M. G. Montgomery, A. G. Leslie, J. E. Walker, How release of phosphate from mammalian F_1-ATPase generates a rotary substep. *Proc. Natl. Acad. Sci. U.S.A.* **112**, 6009–6014 (2015).
25. L. Margulis, M. J. Chapman, Endosymbioses: Cyclical and permanent in evolution. *Trends Microbiol.* **6**, 342–345 (1998).
26. J. J. García-Trejo *et al*., The inhibitory mechanism of the ζ subunit of the F_1F_o-ATPase nanomotor of *Paracoccus denitrificans* and related α-Proteobacteria. *J. Biol. Chem.* **291**, 538–546 (2016).
27. J. A. Pérez, S. J. Ferguson, Kinetics of oxidative phosphorylation in *Paracoccus denitrificans*. 1. Mechanism of ATP synthesis at the active site(s) of F_oF_1-ATPase. *Biochemistry* **29**, 10503–10518 (1990).
28. F. Pacheco-Moisés, F. Minauro-Sanmiguel, C. Bravo, J. J. García, Sulfite inhibits the F_1F_o-ATP synthase and activates the F_1F_o-ATPase of *Paracoccus denitrificans*. *J. Bioenerg. Biomembr.* **34**, 269–278 (2002).
29. T. V. Zharova, A. D. Vinogradov, Proton-translocating ATP-synthase of *Paracoccus denitrificans*: ATP-hydrolytic activity. *Biochem. Biokhimiia* **68**, 1101–1108 (2003).
30. E. Morales-Ríos *et al*., A novel 11-kDa inhibitory subunit in the F_1F_o ATP synthase of *Paracoccus denitrificans* and related alpha-proteobacteria. *FASEB J.* **24**, 599–608 (2010).
31. P. Serrano, M. Geralt, B. Mohanty, K. Wüthrich, NMR structures of α-proteobacterial ATPase-regulating ζ-subunits. *J. Mol. Biol.* **426**, 2547–2553 (2014).
32. M. Zarco-Zavala *et al*., The ζ subunit of the F_1F_o-ATP synthase of α-proteobacteria controls rotation of the nanomotor with a different structure. *FASEB J.* **28**, 2146–2157 (2014).
33. E. Morales-Rios, M. G. Montgomery, A. G. Leslie, J. E. Walker, Structure of ATP synthase from *Paracoccus denitrificans* determined by X-ray crystallography at 4.0 Å resolution. *Proc. Natl. Acad. Sci. U.S.A.* **112**, 13231–13236 (2015).
34. A. Ludlam *et al*., Chaperones of F_1-ATPase. *J. Biol. Chem.* **284**, 17138–17146 (2009).
35. S. H. Ackerman, A. Tzagoloff, Identification of two nuclear genes (ATP11, ATP12) required for assembly of the yeast F_1-ATPase. *Proc. Natl. Acad. Sci. U.S.A.* **87**, 4986–4990 (1990).
36. A. Pícková, M. Potocký, J. Houstek, Assembly factors of F_1F_o-ATP synthase across genomes. *Proteins* **59**, 393–402 (2005).
37. F. Mendoza-Hoffmann *et al*., The biological role of the ζ subunit as unidirectional inhibitor of the F_1F_o-ATPase of *Paracoccus denitrificans*. *Cell Rep.* **22**, 1067–1078 (2018).
38. Y. Hirono-Hara *et al*., Pause and rotation of F_1-ATPase during catalysis. *Proc. Natl. Acad. Sci. U.S.A.* **98**, 13649–13654 (2001).
39. D. G. G. McMillan, R. Watanabe, H. Ueno, G. M. Cook, H. Noji, Biophysical characterization of a thermoalkaliphilic molecular motor with a high stepping torque gives insight into evolutionary ATP synthase adaptation. *J. Biol. Chem.* **291**, 23965–23977 (2016).
40. T. V. Zharova, A. D. Vinogradov, Energy-dependent transformation of F_oF_1-ATPase in *Paracoccus denitrificans* plasma membranes. *J. Biol. Chem.* **279**, 12319–12324 (2004).
41. H. Konno *et al*., The regulator of the F_1 motor: Inhibition of rotation of cyanobacterial F_1-ATPase by the epsilon subunit. *EMBO J.* **25**, 4596–4604 (2006).
42. K. Shimabukuro *et al*., Catalysis and rotation of F_1 motor: Cleavage of ATP at the catalytic site occurs in 1 ms before 40 degree substep rotation. *Proc. Natl. Acad. Sci. U.S.A.* **100**, 14731–14736 (2003).
43. D. Okuno *et al*., Correlation between the conformational states of F_1-ATPase as determined from its crystal structure and single-molecule rotation. *Proc. Natl. Acad. Sci. U.S.A.* **105**, 20722–20727 (2008).
44. Y. Hirono-Hara, K. Ishizuka, K. Kinosita, M. Yoshida, H. Noji, Activation of pausing F_1 motor by external force. *Proc. Natl. Acad. Sci. U.S.A.* **102**, 4288–4293 (2005).
45. S. D. Dunn, R. G. Tozer, V. D. Zadorozny, Activation of *Escherichia coli* F_1-ATPase by lauryldimethylamine oxide and ethylene glycol: Relationship of ATPase activity to the interaction of the epsilon and beta subunits. *Biochemistry* **29**, 4335–4340 (1990).
46. J.-M. Jault *et al*., The $\alpha_3\beta_3\gamma$ complex of the F_1-ATPase from thermophilic *Bacillus PS3* containing the αD261N substitution fails to dissociate inhibitory MgADP from a catalytic site when ATP binds to noncatalytic sites. *Biochemistry* **34**, 16412–16418 (1995).
47. H. R. Lotscher, C. DeJong, R. A. Capaldi, Interconversion of high and low ATPase activity forms of ECF_1 by the detergent lauryldimethylamine oxide. *Biochemistry* **23**, 4140–4143 (1984).
48. K. Hayashi, H. Ueno, R. Iino, H. Noji, Fluctuation theorem applied to F_1-ATPase. *Phys. Rev. Lett.* **104**, 218103 (2010).
49. D. G. McMillan, S. Keis, P. Dimroth, G. M. Cook, A specific adaptation in the a subunit of thermoalkaliphilic F_1F_o-ATP synthase enables ATP synthesis at high pH but not at neutral pH values. *J. Biol. Chem.* **282**, 17395–17404 (2007).
50. P. D. Boyer, A perspective of the binding change mechanism for ATP synthesis. *FASEB J.* **3**, 2164–2178 (1989).
51. P. Mitchell, Molecular mechanics of protonmotive F_oF_1 ATPases: Rolling well and turnstile hypothesis. *FEBS Lett.* **182**, 1–7 (1985).
52. T. M. Duncan, V. V. Bulygin, Y. Zhou, M. L. Hutcheon, R. L. Cross, Rotation of subunits during catalysis by *Escherichia coli* F_1-ATPase. *Proc. Natl. Acad. Sci. U.S.A.* **92**, 10964–10968 (1995).
53. J. Weber, A. E. Senior, Bi-site catalysis in F_1-ATPase: Does it exist? *J. Biol. Chem.* **276**, 35422–35428 (2001).
54. R. Watanabe *et al*., Mechanical modulation of catalytic power on F_1-ATPase. *Nat. Chem. Biol.* **8**, 86–92 (2011).
55. J. J. García, R. A. Capaldi, Unisite catalysis without rotation of the γ-ε domain in *Escherichia coli* F_1-ATPase. *J. Biol. Chem.* **273**, 15940–15945 (1998).
56. J. Pu, M. Karplus, How subunit coupling produces the γ-subunit rotary motion in F_1-ATPase. *Proc. Natl. Acad. Sci. U.S.A.* **105**, 1192–1197 (2008).
57. C. B. Li, H. Ueno, R. Watanabe, H. Noji, T. Komatsuzaki, ATP hydrolysis assists phosphate release and promotes reaction ordering in F_1-ATPase. *Nat. Commun.* **6**, 10223 (2015).
58. S. Mukherjee, A. Warshel, Dissecting the role of the γ-subunit in the rotary-chemical coupling and torque generation of F_1-ATPase. *Proc. Natl. Acad. Sci. U.S.A.* **112**, 2746–2751 (2015).
59. H. Imamura *et al*., Rotation scheme of V_1-motor is different from that of F_1-motor. *Proc. Natl. Acad. Sci. U.S.A.* **102**, 17929–17933 (2005).
60. H. Sielaff *et al*., Power stroke angular velocity profiles of archaeal A-ATP synthase versus thermophilic and mesophilic F-ATP synthase molecular motors. *J. Biol. Chem.* **291**, 25351–25363 (2016).
61. Y. Minagawa *et al*., Basic properties of rotary dynamics of the molecular motor *Enterococcus hirae* V_1-ATPase. *J. Biol. Chem.* **288**, 32700–32707 (2013).
62. S. Furuike *et al*., Resolving stepping rotation in *Thermus thermophilus* H^+-ATPase/synthase with an essentially drag-free probe. *Nat. Commun.* **2**, 233 (2011).
63. T. Iida *et al*., Single-molecule analysis reveals rotational substeps and chemomechanical coupling scheme of *Enterococcus hirae* V_1-ATPase. *J. Biol. Chem.* **294**, 17017–17030 (2019).
64. H. Noji, H. Ueno, R. Kobayashi, Correlation between the numbers of rotation steps in the ATPase and proton-conducting domains of F-and V-ATPases. *Biophys. Rev.* **12**, 303–307 (2020).
65. I. Watt, M. Montgomery, M. Runswick, A. Leslie, J. Walker, Bioenergetic cost of making an adenosine triphosphate molecule in animal mitochondria. *Proc. Natl. Acad. Sci. U.S.A.* **107**, 16823–16827 (2010).
66. H. Guo, T. Suzuki, J. L. Rubinstein, Structure of a bacterial ATP synthase. *eLife* **8**, e43128 (2019).
67. M. Sobti *et al*., Cryo-EM structures of the autoinhibited *E. coli* ATP synthase in three rotational states. *eLife* **5**, e21598 (2016).

68. W. C. Y. Lau, J. L. Rubinstein, Structure of intact *Thermus thermophilus* V-ATPase by cryo-EM reveals organization of the membrane-bound V_o motor. *Proc. Natl. Acad. Sci. U.S.A.* **107**, 1367–1372 (2010).
69. T. Murata, I. Yamato, Y. Kakinuma, A. G. W. Leslie, J. E. Walker, Structure of the rotor of the V-type Na^+-ATPase from *Enterococcus hirae*. *Science* **308**, 654–659 (2005).
70. T. Meier, P. Polzer, K. Diederichs, W. Welte, P. Dimroth, Structure of the rotor ring of F-Type Na^+-ATPase from *Ilyobacter tartaricus*. *Science* **308**, 659–662 (2005).
71. S. Saroussi, M. Schushan, N. Ben-Tal, W. Junge, N. Nelson, Structure and flexibility of the C-ring in the electromotor of rotary F_oF_1-ATPase of pea chloroplasts. *PLoS One* **7**, e43045 (2012).
72. D. Pogoryelov, Ö. Yildiz, J. D. Faraldo-Gómez, T. Meier, High-resolution structure of the rotor ring of a proton-dependent ATP synthase. *Nat. Struct. Mol. Biol.* **16**, 1068 (2009).
73. L. Preiss *et al*., Structure of the mycobacterial ATP synthase F_o rotor ring in complex with the anti-TB drug bedaquiline. *Sci. Adv.* **1**, e1500106 (2015).
74. F. Varghese, J. N. Blaza, A. J. Y. Jones, O. D. Jarman, J. Hirst, Deleting the IF_1-like ζ subunit from *Paracoccus denitrificans* ATP synthase is not sufficient to activate ATP hydrolysis. *Open Biol.* **8**, 170206 (2018).
75. M. Zarco-Zavala, F. Mendoza-Hoffmann, J. J. García-Trejo, Unidirectional regulation of the F_1F_o-ATP synthase nanomotor by the ζ pawl-ratchet inhibitor protein of *Paracoccus denitrificans* and related α-proteobacteria. *Biochim. Biophys. Acta Bioenerg.* **1859**, 762–774 (2018).
76. D. J. Klionsky, W. S. Brusilow, R. D. Simoni, *In vivo* evidence for the role of the epsilon subunit as an inhibitor of the proton-translocating ATPase of *Escherichia coli*. *J. Bacteriol.* **160**, 1055–1060 (1984).
77. R. Watanabe, R. Iino, H. Noji, Phosphate release in F_1-ATPase catalytic cycle follows ADP release. *Nat. Chem. Biol.* **6**, 814–820 (2010).